



A proficient microwave synthesis with structure elucidation and the exploitation of the biological behavior of the newly halogenated 3-amino-1*H*-benzo[*f*]chromene molecules, targeting dual inhibition of topoisomerase II and microtubules

Ahmed M. Fouda^a, Rawda M. Okasha^b, Fawzia F. Alblewi^b, Ahmed Mora^c, Tarek H Afifi^b,
Ahmed M. El-Agrody^{c,*}

^a Chemistry Department, Faculty of Science, King Khalid University, Abha 61413, Saudi Arabia

^b Chemistry Department, Faculty of Science, Taibah University, Al-Madinah Al-Munawarah 30002, Saudi Arabia

^c Chemistry Department, Faculty of Science, Al-Azhar University, Nasr City 11884, Cairo, Egypt

ARTICLE INFO

Keywords:

Benzochromenes
Antitumor activity
Cell cycle analysis
Caspases
Topoisomerase
DNA fragmentation
SAR study

ABSTRACT

In our endeavors to develop novel and powerful agents with antiproliferative activities, a series of β -enamionitriles, linked to the 8-bromo-1*H*-benzo[*f*]chromene moieties (**4a-m**), was designed and synthesized under microwave irradiation conditions. The structures of the target compounds were established on the basis of their spectral data: IR, ¹H NMR, ¹³C NMR, ¹³C NMR-DEPT/APT, ¹⁹F NMR and MS. Furthermore, the antiproliferative properties were evaluated against the human cancer cell lines MCF-7, HCT-116, and HepG-2 in comparison to the positive controls Vinblastine and Doxorubicin, employing the viability assay. The obtained results confirmed that most of the tested molecules revealed strong and selective cytotoxic activities against the three cancer cell lines. The most potent cytotoxic compounds **4b**, **4d**, **4e**, **4i**, and **4k** were elected for further examination, such as the cell cycle analysis, the apoptosis assay, the Caspase production, and the DNA fragmentation. This study also revealed that the desired compounds stimulate cell cycle arrest at the G2/M phases, increase the production of Caspases 3, 8, and 9, and finally cause intrinsic and extrinsic apoptotic cell death. Moreover, these compounds suppress the action of the topoisomerase II enzyme and also disrupt the microtubule functions. The SAR study of the synthesized compounds verified that the substitution on the phenyl ring of the 1*H*-benzo[*f*]chromene nucleus, accompanied with the presence of the bromine atom at the 8-position, increases the ability of these molecules against different cell lines.

1. Introduction

Chromene and benzochromene derivatives perform vital roles in many biological processes, such as antimicrobial [1–4] anti-influenza virus [5] antiproliferative [6–8] anticancer [9] anti-inflammatory [10,11] antitubercular [12,13] Alzheimer disease [14] and anti-obesity [15] effects and agents. A large number of the chromene derivatives have been prepared with interesting anticancer properties, and several examples have exhibited cytotoxic effects on cancer related cell lines in the micro/nano-molar concentration range. For example, the 6-aryl-4*H*-chromene derivatives (**A**) acted as stable and ROS-free antagonistic, antiapoptotic Bcl-2 proteins [16,17]; the C4-*N,N*-dialkyl-aniline-substituted 4-aryl-4*H*-chromene derivatives (**B**) contain antiproliferative properties against the tumor cell lines, namely: hepatocellular

carcinoma (HepG-2), cervical cancer (HeLa), and lung adenocarcinoma (A549) [18]. The 7-(dimethylamino/amino/hydroxy)-4-(5/4-nitrothiophen-2-yl)-4*H*-chromene and the 2,7,8-triamino-4-(5-nitrothiophen-2-yl)-4*H*-chromene derivatives (**C**) operated as the inducers of apoptosis [19]; the ethyl 2-amino-6-bromo-4-(1-cyano-2-ethoxy-2-oxoethyl)-4*H*-chromene-3-carboxylate (HA 14-1) (**D**) performed as an inhibitor of the Bcl-2 proteins [20], which also demonstrated selective cytotoxicity against drug-resistant cancer cells that overexpress the antiapoptotic Bcl-2 family proteins [21,22]. The ethyl 4-((ethoxycarbonyl)methyl)-2-amino-6-phenyl-4*H*-chromene-3-carboxylate (sHA 14-1) (**E**) displayed synergism and selective toxicity against the Bcl-2-overexpressing drug-resistant cancer cells [23], and ethyl 2-amino-4-(2-morpholino-2-oxoethyl)-6-phenyl-4*H*-chromene-3-carboxylate (isHA 14-1) (**F**) acted as an inhibitor of the Bcl-2 protein [17] as

* Corresponding author.

E-mail addresses: elagrody_am@yahoo.com, ahm1954@hotmail.com, elagrody_am47@gmail.com (A.M. El-Agrody).

<https://doi.org/10.1016/j.bioorg.2019.103549>

Received 10 October 2019; Received in revised form 17 December 2019; Accepted 21 December 2019

Available online 23 December 2019

0045-2068/ © 2019 Elsevier Inc. All rights reserved.

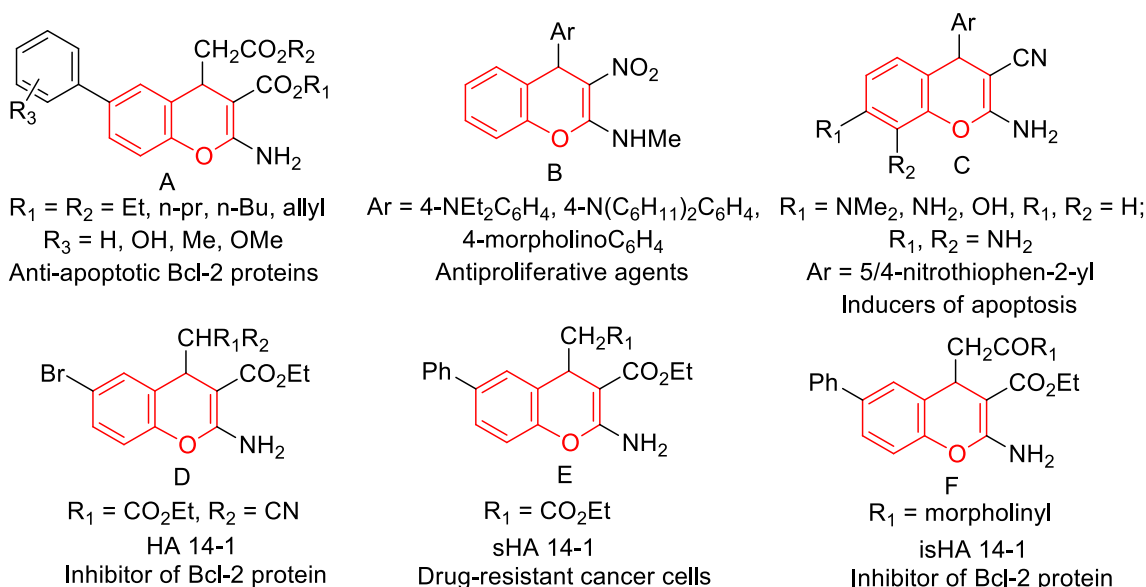


Fig. 1. Chromene drugs (Red highlighted) with different biological activities.

shown in (Fig. 1).

Furthermore, the benzochromene derivatives are a very efficacious choice for the treatment of several human diseases. For instance, the 3-amino-1-aryl-8-bromo-1*H*-benzo[*f*]chromenes (G) and the 3-amino-1-aryl-8-methoxy-1*H*-benzo[*f*]chromenes (H) demonstrated high potency for the cell invasion assay, the caspase 3/7 assay, and the *c-Src* kinase inhibitors [24]. The 3-amino-1-aryl-1*H*-benzo[*f*]chromene-2-carbonitriles (I) exhibited *c-Src* kinase inhibitory and antiproliferative activities [25] while the 2-amino-5,6-dihydro-4-aryl-4*H*-benzo[*h*]chromene-3-carbonitriles (J) has good antiproliferative activities against different cell lines [26]. Additionally, the 2-amino-4-aryl-4*H*-benzo[*h*]chromene-2-carbonitriles (K) revealed *c-Src* kinase inhibitory and antiproliferative activities [25] and the 2-amino-4-aryl-8-methoxy-4*H*-benzo[*h*]chromene-2-carbonitriles (L) performed as a potent anticancer analog and targeted the *c-Src* Kinase enzyme [27] as presented in (Fig. 2).

In the present study, the β -enamionitriles, linked to the 8-bromo-1*H*-

benzo[*f*]chromene moieties, were synthesized, and their anti-proliferative activities were surveyed against three cancer cell lines: MCF-7, HCT-116, and HepG-2. Moreover, the most potent prepared compounds targeted both the topoisomerase II and microtubules, eliciting a cell cycle arrest at the G2/M phases and the induction of the caspase dependent apoptosis. The structure activity relationships (SARs) disclose that the introduction of certain lipophilic halogen substituents on the phenyl ring, attached to the 1-position of the 8-bromo-1*H*-benzo[*f*]chromene moiety, enhanced the antitumor activities.

2. Results and discussion

2.1. Chemistry

The β -enamionitriles (4a-m), attached to the 8-bromo-1*H*-benzo[*f*]

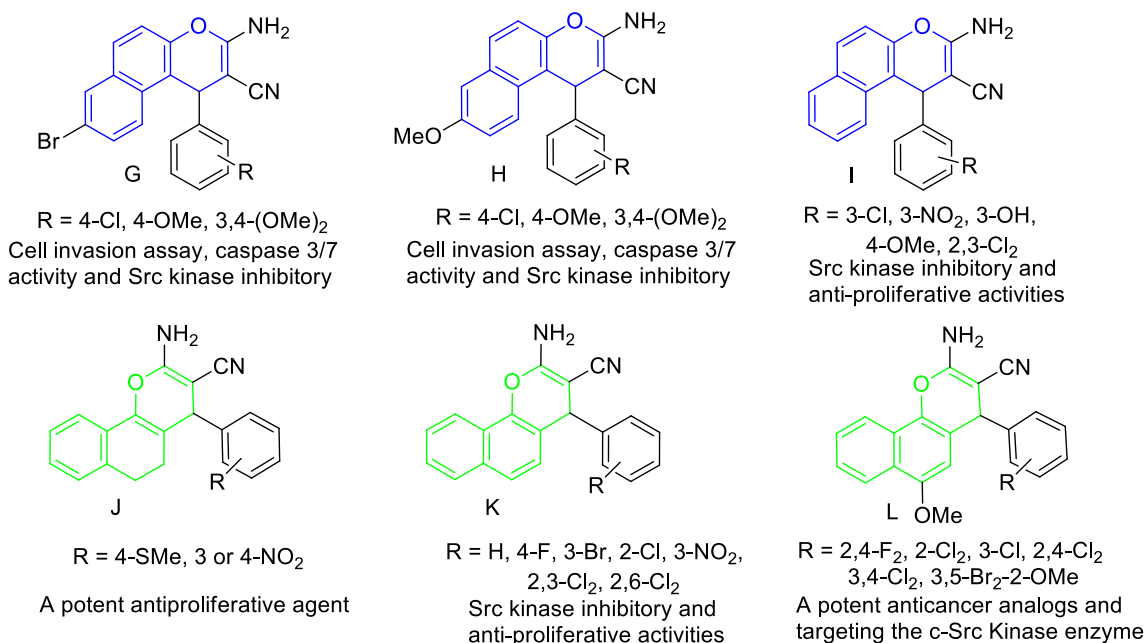
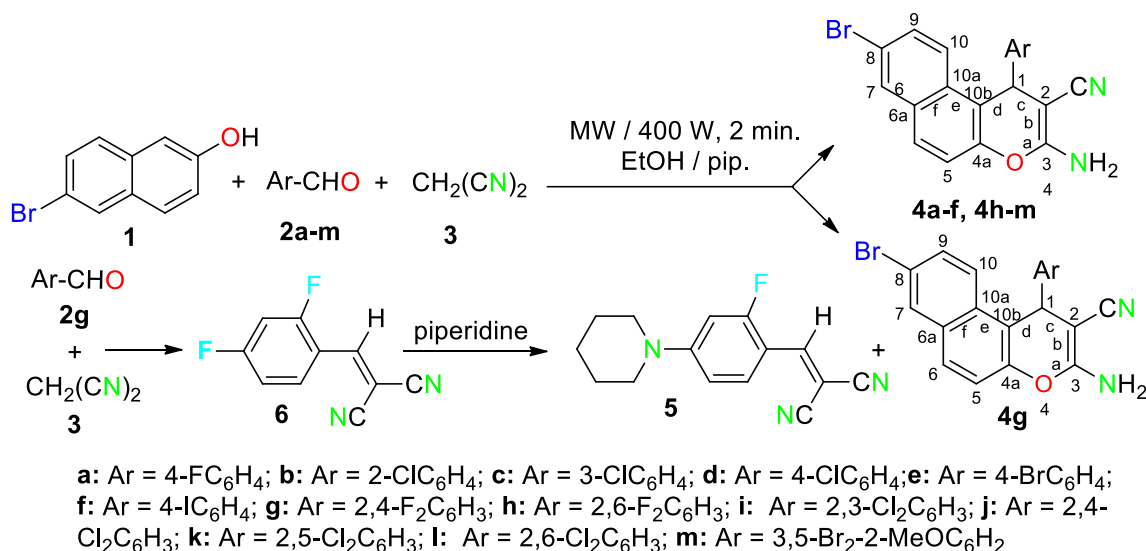


Fig. 2. Structure of some 1*H*-benzo[*f*]chromene derivatives (blue highlighted) and 4*H*-benzo[*h*]chromene derivatives (Green highlighted) with cytotoxic and apoptotic effects.



Scheme 1. Synthesis of halogenated 1H-benzo[f]chromene derivatives (4a-m) and 2-(2-fluoro-4-(piperidin-1-yl)benzylidene)malononitrile (5).

chromene groups, were synthesized, as represented in (Scheme 1). The halogenated phenyl ring at the 1-position of the 3-amino-8-bromo-1H-benzo[f]chromene-2-carbonitriles (4a-m) was easily acquired in a good yield by the condensation of 6-bromo-2-naphthol (1) with the appropriate aromatic aldehydes (2a-m) and malononitrile (3) in an ethanolic piperidine solution employing microwave irradiation for 2 min. at 140 °C. In addition, compound 2-(2-fluoro-4-(piperidin-1-yl)benzylidene)malononitrile (5) was unintentionally formed as side product via the exploitation of 2,4-difluorobenzylidenemalononitrile (6). The maximum power of the microwave irradiation was optimized by repeating the reaction at different watt powers and periods of time, which delivered the ideal condition at 400 W and reaction time 2 min. and provided the highest yield of the desired compounds. It is also critical to remark that the 1-position of compounds 4a-m is a chiral center.

The unexpected formation of compound 5 proceeds simply via the displacement of the fluorine atom at the formed 2,4-difluorobenzylidenemalononitrile (6) by the piperidinyl moiety via a nucleophilic aromatic substitution reaction at the 4-position rather than the 2-position due to the steric hindrance of the fluorine atom at the 2-position, (Scheme 1). Further, the structure of the 2-(2-fluoro-4-(piperidin-1-yl)benzylidene)malononitrile (5) was supported by an independent synthesis of the same compound through the nucleophilic substitution of the fluorine atom at the 4-position of 2g with piperidine to give 2-fluoro-4-piperidin-1-yl-benzaldehyde (7), followed by the condensation of 7 with malononitrile (3) in an ethanol solution under reflux conditions, as illustrated in (Scheme 2).

The characterization of the synthesized compounds using the spectroscopic data (IR, ¹H/¹³C NMR, ¹⁹F NMR, ¹³C NMR-DEPT/APT, MS, X-ray) and the elemental analyses were consistent with their structures. The IR spectra of 4a-m exhibited characteristic absorption bands around ν 3479–3443, 3338–3320, 3290–3189 cm⁻¹, due to the amino groups while the nitrile groups' functionality in 4a-m was detected to be in the range of ν 2203–2190 cm⁻¹. The ¹H NMR spectra of compounds 4a-m displayed singlet signals, resonating around δ

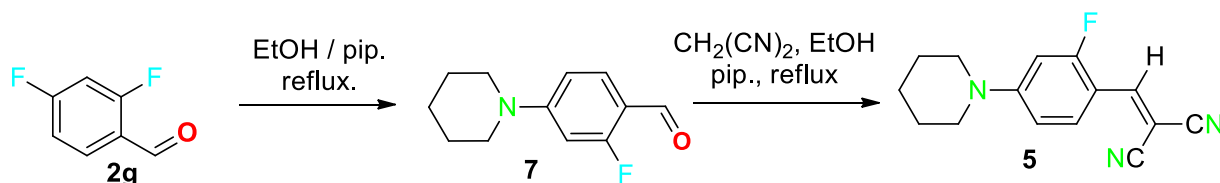
7.18–7.02 ppm, which were representing the amino groups' protons, and at δ 6.11–5.35, which were attributable to the methine protons of the heterocyclic ring. Meanwhile, the ¹³C NMR spectra of 4a-m showed the corresponding methine carbons around δ 37.16–27.96 ppm. Additionally, the IR spectrum of compound 5 revealed an absorption band at ν 2212 cm⁻¹ for the CN group, while the ¹H NMR and ¹³C NMR spectra of 5 presented the signals of the olefinic proton and carbon at δ 7.86 ppm and δ 149.97 ppm, respectively. Furthermore, the MS spectra of 4a-m and 5, the ¹³C NMR-DEPT/APT of compound 4a and 5, ¹⁹F NMR of compound 5 and the single crystal X-ray analysis of compound 4k [28] as a representative example, gave an absolute confirmation for the target structures.

2.2. Biological activity

2.2.1. In vitro cytotoxic activity

Based on the importance of benzochromene (16–24) as antitumor agents, we designed halogenated 3-amino-1H-benzo[f]chromenes molecules with various aryl substitutions. The MTT assay [29–31] was performed to evaluate the cytotoxic effects of these halogenated 3-amino-1H-benzo[f]chromene derivatives (4a-m) against the selected human cancer cell lines, namely: mammary gland breast cancer (MCF-7), human colon cancer (HCT-116), and human hepatocellular carcinoma (HepG-2), utilizing Doxorubicin and Vinblastine as reference compounds. The *in-vitro* cytotoxicity evaluation was achieved under different concentrations, expressed as growth inhibitory concentration (IC₅₀) values, (Table 1) and (Fig. 3).

Interestingly, the results revealed that most the synthesized halogenated 3-amino-1H-benzo-[f]chromene derivatives (4a-m) exhibited excellent to good antiproliferative activity as comparison with the standard drugs (Doxorubicin and Vinblastine). Among these derivatives, 4d, 4b, 4i, 4k, 4g, 4e, 4l, 4m, 4h, and 4a with IC₅₀ values in the range of 0.5–5.2 μ g/mL, respectively, were found to be the most potent of all the assessed compounds against the MCF-7 in comparison with



Scheme 2. Synthesis of 2-(2-fluoro-4-(piperidin-1-yl)benzylidene)malononitrile (5) via 2-fluoro-4-piperidin-1-yl-benzaldehyde (7).

Table 1
IC₅₀ values of the target compounds against MCF-7, HCT-116 and HepG-2 cell lines.

Compound	Ar	IC ₅₀ (μg/mL) ^a		
		MCF-7	HCT-116	HepG-2
4a	4-FC ₆ H ₄	5.2 ± 0.03 ^b	1.0 ± 0.12 ^b	0.8 ± 0.12 ^b
4b	2-ClC ₆ H ₄	1.0 ± 0.16	1.46 ± 0.35	1.1 ± 0.5
4c	3-ClC ₆ H ₄	8.3 ± 0.14	6.0 ± 0.14	5.2 ± 0.2
4d	4-ClC ₆ H ₄	0.5 ± 0.23 ^b	0.7 ± 0.11 ^b	1.1 ± 0.12 ^b
4e	4-BrC ₆ H ₄	2.5 ± 0.14 ^b	0.5 ± 0.35 ^b	1.8 ± 0.02 ^b
4f	4-IC ₆ H ₄	59.7 ± 0.2	30.5 ± 0.7	20.0 ± 0.11
4g	2,4-F ₂ C ₆ H ₃	1.7 ± 0.2	1.36 ± 0.12	2.0 ± 0.12
4h	2,6-F ₂ C ₆ H ₃	4.8 ± 0.1	0.5 ± 0.17	1.1 ± 0.21
4i	2,3-Cl ₂ C ₆ H ₃	1.0 ± 0.02	2.4 ± 0.15	1.3 ± 0.14
4j	2,4-Cl ₂ C ₆ H ₃	32.0 ± 0.01	0.7 ± 0.23	0.6 ± 0.03
4k	2,5-Cl ₂ C ₆ H ₃	1.0 ± 0.06	0.6 ± 0.16	0.7 ± 0.18
4l	2,6-Cl ₂ C ₆ H ₃	2.8 ± 0.4	8.7 ± 0.01	2.9 ± 0.02
4m	3,5-Br ₂ -2-OMeC ₆ H ₂	3.6 ± 0.15	2.8 ± 0.6	1.54 ± 0.13
Vinblastine	-	6.1 ± 0.03	2.6 ± 0.08	4.6 ± 0.01
Doxorubicin	-	0.4 ± 0.01	0.5 ± 0.015	0.9 ± 0.04

^a IC₅₀ values expressed in μg/mL as the mean values of triplicate wells from at least three experiments and are reported as the mean ± standard error.

^b [24].

Vinblastine (IC₅₀ = 6.1 μg/mL). Compound **4d** (IC₅₀ = 0.5 μg/mL) was almost equipotent as Doxorubicin (IC₅₀ = 0.4 μg/mL) and emerged as the most potent counterpart against MCF-7 in this study. Additionally, compounds **4h**, **4e**, **4k**, **4d**, **4j**, **4a**, **4g**, **4b**, and **4i** (IC₅₀ = 0.5–2.4 μg/mL) possessed excellent antiproliferative activities against the HCT-116 cells, which proved to excel further than the employed reference drug Vinblastine (IC₅₀ = 2.6 μg/mL), and compounds **4h**, **4e**, **4k**, **4d**, and **4j** displayed less anti-proliferative activities than or equipotent as Doxorubicin with IC₅₀ values, ranging from 0.5 to 0.7 μg/mL. The derivatives **4j**, **4k**, **4a**, **4h**, **4b**, **4d**, **4i**, **4m**, **4e**, **4g**, and **4l** demonstrated superior activities against the HepG-2 cell line with IC₅₀ of 0.6–2.9 μg/mL as compared to Vinblastine (IC₅₀ = 4.6 μg/mL) while compounds **4j**, **4k**, and **4a** (IC₅₀ = 0.6–0.8 μg/mL) were discovered to be the most potent counterpart in evaluation with Doxorubicin (IC₅₀ = 0.9 μg/mL). Lastly, derivatives **4h**, **4b**, and **4i** (IC₅₀ = 1.1–1.3 μg/mL) were almost equipotent as Doxorubicin.

2.2.2. Cell cycle distribution at G2/M phase

The four cell cycle stages (G1, S, G2, and M) ensure a controlled

normal cell growth and division; however, most cancer cells undergo unscheduled cell divisions by the down regulation of the cell cycle. Therefore, the newly synthesized anticancer derivatives, inhibiting the cell cycle, represent a critical therapeutic intervention in treating proliferative diseases like cancer [32,33]. To determine whether the potent cytotoxicity experienced by the novel compounds (**4b**, **4d**, **4e**, **4i**, and **4k**) was due to the inhibitory effect on the cell cycle process, the DNA content was analyzed by the flow cytometry, utilizing the FACS Calibur (Becton Dickinson). The MCF-7, HCT-116, and HepG-2 cells were remedied with each derivative at its IC₅₀ value for 24 h; moreover, a controlled experiment with no treatment was incorporated as shown in the representative cell cycle distribution histograms of the stained DNA in (Fig. 4a). The results on regulating the cell cycle progression demonstrated that all the examined compounds induced a significant increase in the cell population arrest at the G2/M phases with a decreased cell count in the G1 and S phases, as portrayed in (Fig. 4b). The cell cycle evaluation established that the analyzed derivatives substantially arrested the cells' progression by restricting the G2/M phases.

2.2.3. Induction of apoptosis by the newly synthesized compounds

To further assess whether the tumor suppression property of the tested compounds was due to apoptotic cell death, the Annexin V/PI double staining flow cytometric assay was applied to determine whether the phosphatidylserine (PS) translocation appeared on the membrane surface as an accepted marker for apoptosis [34]. The representative dot plots of the double stained cells (MCF-7, HCT-116, and HepG-2), after treatment with the investigated compounds, were revealed in (Fig. 5a). Unlike necrosis, which was not detected, all the remedied cells revealed an increase from 10 to 25% in total apoptosis in comparison to the untreated cells. However, compounds **4d** and **4k** disclosed higher apoptosis percentages in the case of the MCF-7 (24%) and HCT-116 (25%) cells when assessed against the HepG-2 (14%) cells, (Fig. 5b, c, and d). When evaluated against the vehicle's controls, the treated cells with compound **4e** experienced an increase in a stage of early apoptosis (Annexin V positive, PI negative) by a 4, 11, and 9 for MCF-7, HCT-116, and HepG-2, respectively while the late apoptosis (Annexin V positive, PI positive) was 27, 16, and 53 for MCF-7, HCT-116, and HepG-2 cells, respectively, Fig. 5e. In another report, the Annexin V single positive cells emerged only after treatment with early anticancer drugs such as Etoposide and Cytarabine, but this did not occur with the late anticancer drugs such as Doxorubicin and Methotrexate [35,36]. The results insinuated that the desired molecules, performing as drug candidates, exhibited more potent cytotoxicity during the induction of late apoptosis.

2.2.4. Increased protein levels of Caspases 3, 8, and 9

The Caspases' members of the cysteine proteases family trigger apoptosis through an extrinsic pathway, associated with the activation of

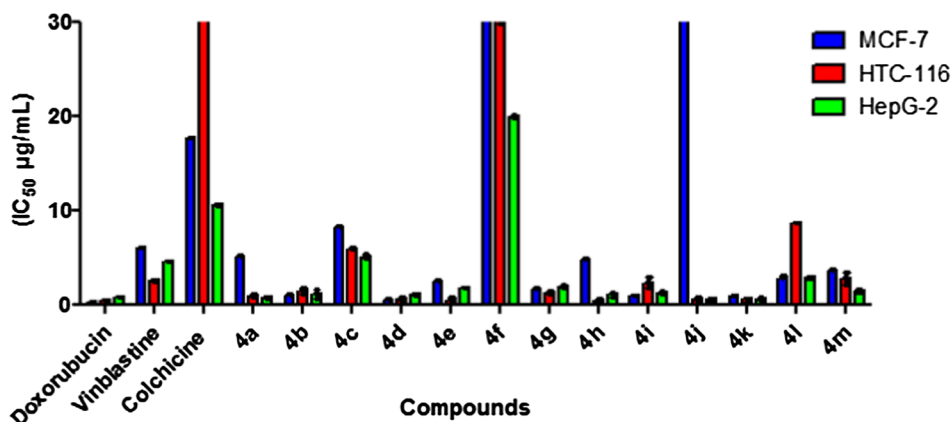


Fig. 3. IC₅₀ values expressed in (μg/mL) of halogenated 1H-benzo[f]chromene derivatives **4a-m** against MCF-7, HCT-116 and HepG-2 tumor cells.

the initiator Caspase-8, or an intrinsic pathway, allied with the activation of the initiator Caspase-9, which finally stems the activation of the executioner Caspases such as Caspase-3 [37,38]. Furthermore, the protein levels of Caspase-3, Caspase-8, and Caspase-9 were measured, exploiting the enzyme-linked immunosorbent assay in the different remedied tumor cells (Fig. 6a, b, and c), to further verify the impact of the analyzed

derivatives on the apoptotic pathway. Fig. 6d illustrates the fold change for each of the Caspases after their therapy with the examined cancer cells and compound 4e for 24h in assessment with the suggested control cells. The up regulation of Caspase-8 and Caspase-9 suggested that the newly synthesized compounds stimulated apoptosis via the extrinsic/death receptors and the intrinsic/mitochondrial pathway. Our results are

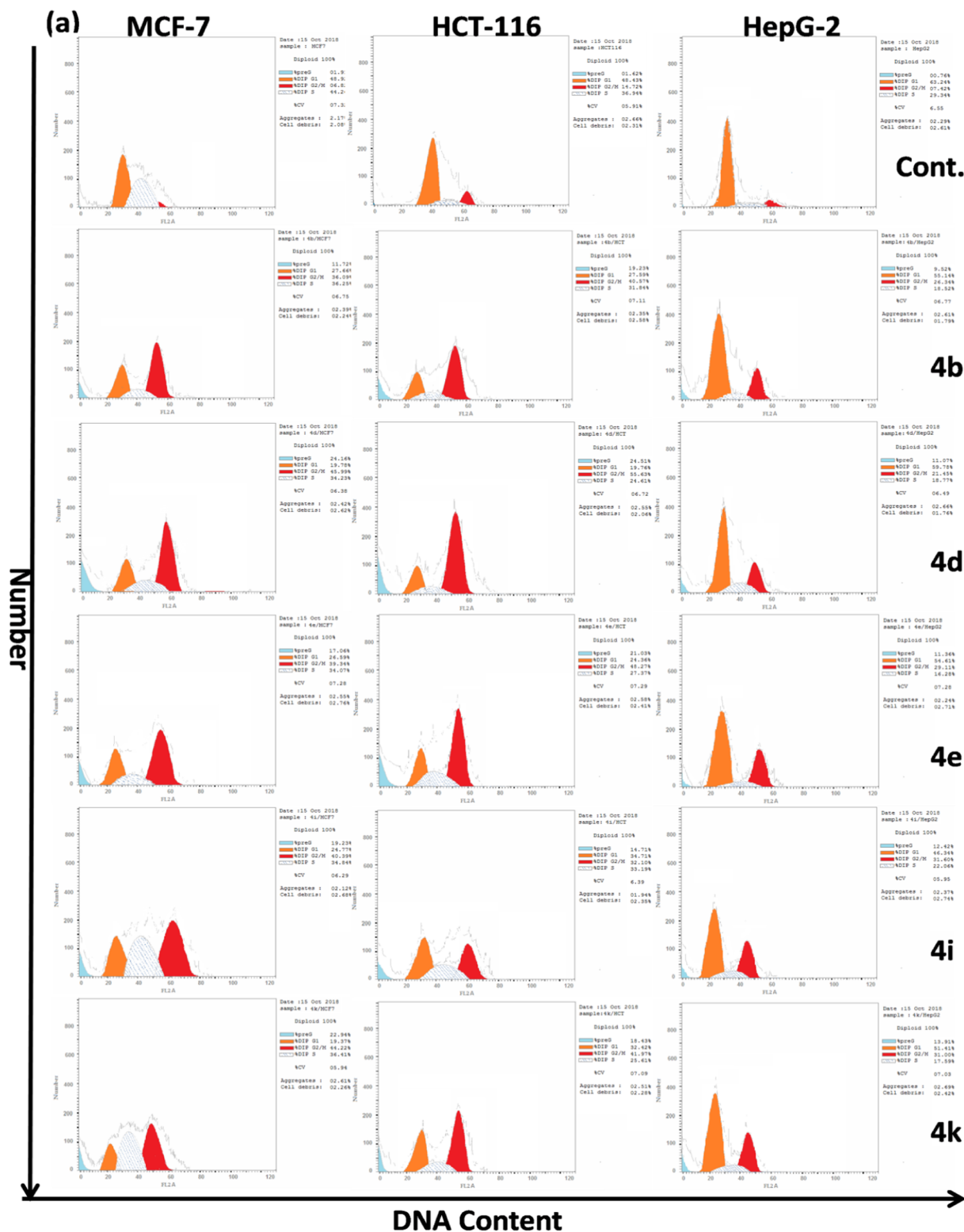


Fig. 4. The induced cell cycle arrest at the G2/M phase. (a) The representative flow cytometry histograms of the cell cycle distribution. The DNA content was stained with (PI). (b) the percentage of MCF-7, HCT-116 and HepG-2 cells in the G1, S, and G2/M phases after incubation with compounds 4b, 4d, 4e, 4i, and 4k (IC₅₀ values) for 24 h.

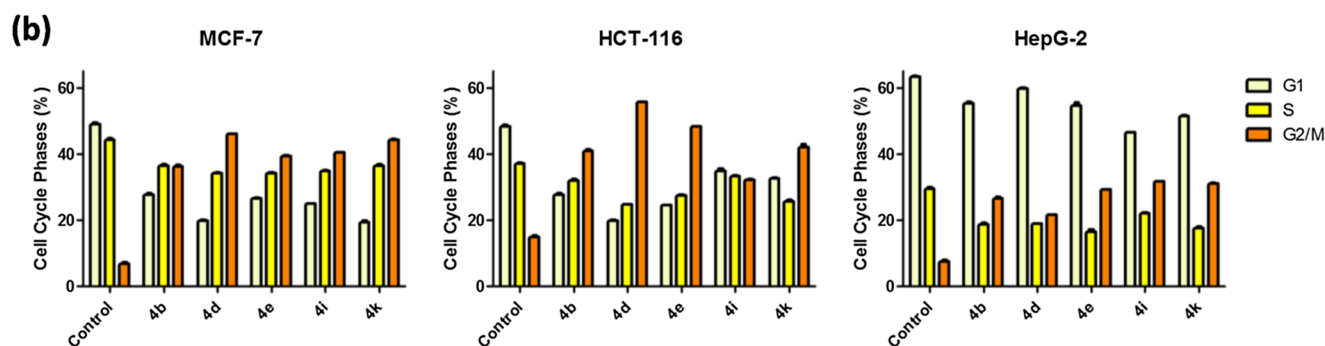


Fig. 4. (continued)

in accordance with previous reports, demonstrating that the Bleomycin, Doxorubicin, and Mitoxantrone anticancer agents are involved in the activation of both the extrinsic as well as the intrinsic apoptotic pathways, which is accompanied by an increased enzymatic activity of Caspases (Caspase-3, Caspase-8, and Caspase-9) [39].

2.2.5. Production of apoptotic DNA fragmentation

The presence of Caspase-3 is associated with the typical hallmarks of apoptosis such as DNA fragmentation [40]. Therefore, the relative quantity of DNA fragments were detected, employing the diphenylamine (DPA) reagent in the different cancer cells, remedied with compounds 4b, 4d, 4e, 4i, 4k, and Doxorubicin 24 h. The percentage of DNA fragmentation in all tumor cells, nursed with our yielded derivatives, was double the attained percentage by the cells treated with the reference drug Doxorubicin, (Fig. 7). These results integrated with the Caspases' levels are formerly demonstrated.

2.2.6. Inhibition of Topoisomerase II

Recently, the cell cycle checkpoint arrest has been exercised as a novel approach to amplify the efficacy and specify the conventional chemotherapy [41]. In the preceding reports, it was established that the topoisomerase II inhibitors trigger the G2/M phases arrest due to the absolute failure of the chromosome decatenation procedure [42,43]. However, it was confirmed that all the new desired molecules prompt cell cycle arrest at the G2/M phase in the dissimilar tumor lines. Thus, the possible inhibitory effect for each derivative was explored for the topoisomerase II activity, exploiting the plasmid-based Topoisomerase II assay. The capability of the topoisomerase II enzymes to decatenate the supercoiled plasmid DNA into a relaxed form experienced no activity with compound 4b, weak activity with compounds 4e and 4i, and the strongest inhibitory effect in regards to compounds 4d and 4k, which is equivalent to the Doxorubicin standard drug, (Fig. 8). Additionally, the gained outcomes elucidated the role of the assessed molecules in the inhibition of Topoisomerase II and the interruption of a vital cell cycle stage, consequently leading to cell death. These results are in accordance with Magar *et al.* work, illustrating the effective inhibition of the Topoisomerase II by the produced chromene analogues as selective targeting anticancer agents [44]. Furthermore, a number of antitumor drugs (Doxorubicin and Etoposide) were scrutinized for their cytotoxicity, due to their ability to stabilize a covalent Topoisomerase II-DNA intermediate [45].

2.2.7. Inhibition of microtubules

Microtubules are major components of the eukaryotic cytoskeleton that result from the interaction of the alpha and beta tubulins polymers. Microtubules perform sundry functions in cells, including mitosis; therefore, the disruption of microtubules generates cell cycle arrest in the G2/M phases and apoptosis, rendering it an attractive target for new anticancer drugs [46,47]. The possible depolymerization effects of the most potent cytotoxic molecules were investigated, employing the preformed microtubules in a free cell system. Enhanced concentrations

(0–10 μ M) of the analyzed compounds were added to the preformed microtubules suspensions to monitor the decrease in the fluorescence intensity, measured as a sign for depolymerization. All the assessed compounds stimulated rapid depolymerization of the previously developed microtubules in a concentration-dependent fashion, denoted by the decrease in the fluorescence values when evaluated against the Colchicine reference drug, (Fig. 9a). The percentages of the microtubules polymerization inhibition at a 10 μ M concentration were 47, 55, and 57 for compounds 4e, 4k, and Colchicine, respectively. In addition, the remaining examined derivatives destabilize the microtubules formation by 40%, as depicted in (Fig. 9b). Based on the mechanism of action, the microtubule inhibitors are usually classified as stabilizer (paclitaxel and docetaxel) or destabilizer (Vinblastine and Colchicine) agents [48]. In this existing report, our molecules demonstrated the inhibition of the microtubules polymerization by destabilizing the preformed tubulin polymer. Furthermore, all the combined outcomes signify that the cultivated derivatives (4d, 4e, 4i, and 4k) firstly targeted the topoisomerase II and microtubules. Consequently, the inhibition of the topoisomerase II and microtubules detain cells at the G2/M phases and, subsequently, activate extrinsic and intrinsic caspase-dependent apoptosis, which is ensued by DNA fragmentation and the proliferation inhibition of cancer cells, Fig. 9c.

2.3. SAR studies

The SAR study revealed several crucial structural requirements, which enhanced the potency of these halogenated 3-amino-1H-benzo[f]chromene derivatives (4a-m). By exemplifying the variations in the substitution pattern on the phenyl ring at the 1-position of the benzo[f]chromene moiety, the molecules possessing electron-withdrawing and electron-donating substituents were prepared with their effects being analyzed. It is noteworthy to observe that the halogenated monosubstituents (first series) on the phenyl ring of compounds 4a-f have a significant impact on the activities against the MCF-7 cell line in evaluation against Vinblastine and Doxorubicin, where the activities were decreased in the order of 4-Cl > 2-Cl > 4-Br > 4-F > 3-Cl > 4-I. Moreover, for the halogenated disubstituents (second series) on the phenyl ring of the molecules 4g-l, the order of the antiproliferative activities is widely varied in accordance to the position and the size of the halogenated disubstituents on the phenyl ring of the benzo[f]chromene moiety; subsequently, the activities were decreased in the order 2,3-Cl₂ > 2,5-Cl₂ > 2,4-F₂ > 2,6-Cl₂ > 2,6-F₂ > 2,4-Cl₂. The trisubstituent (third series) like 3,5-Br₂-2-OME of compound 4m demonstrated good activity, as compared to Vinblastine, hinting that the grafting of the lipophilic electron-withdrawing monosubstituents is more beneficial than that of the disubstituents and trisubstituents. Additionally, the moderate size of the lipophilic electron-withdrawing disubstituents, similar to 2,3-Cl₂; 2,5-Cl₂; and 2,4-F₂, displayed more activity than the other disubstituents and trisubstituents, respectively. Regarding the activity against the HCT-116 line, molecules 4h, 4e, 4k, 4d, 4j, 4a, 4g, 4b, and 4i were the most effectual analogs through this

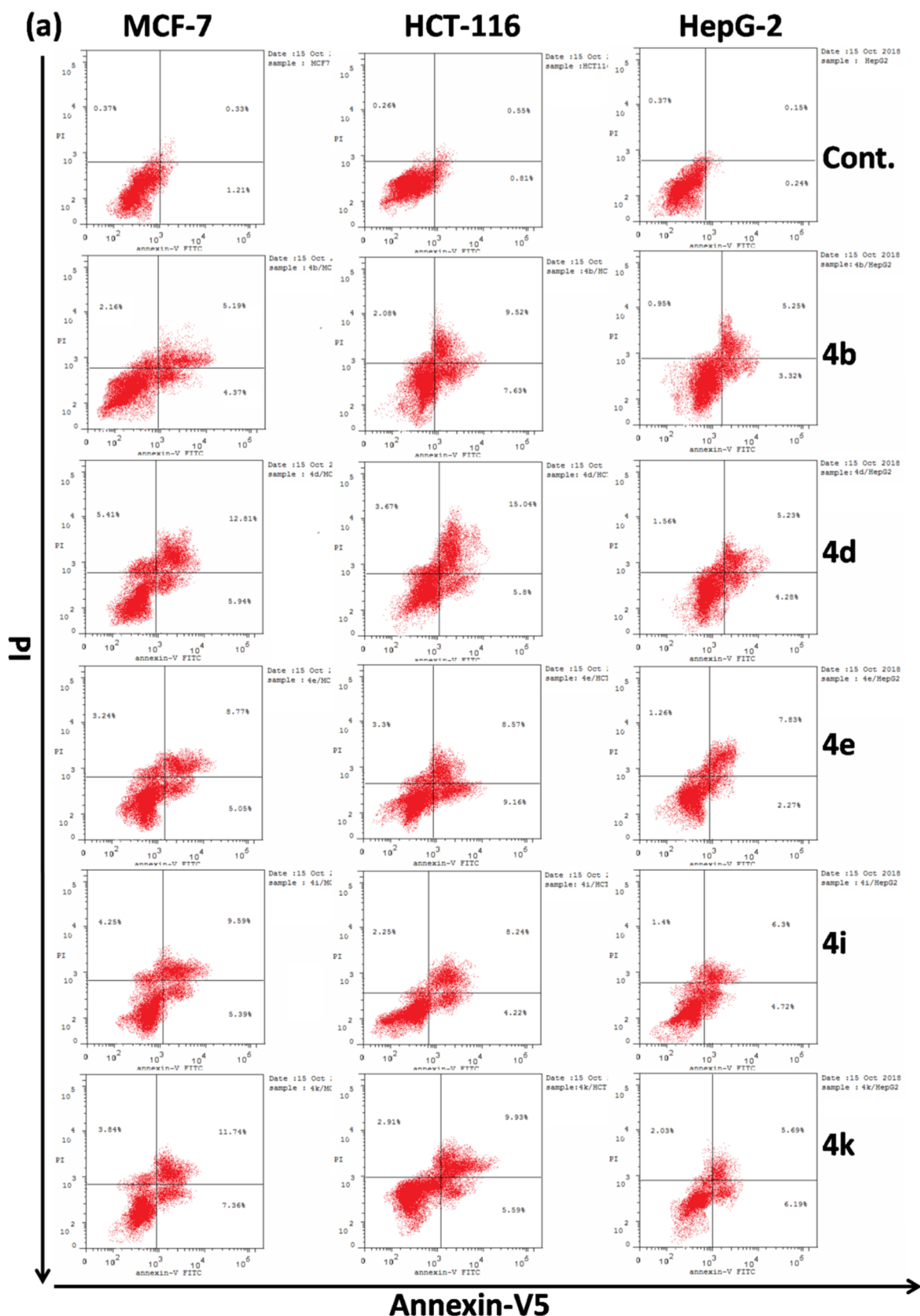


Fig. 5. Apoptotic cell death induced by the halogenated 1*H*-benzo[*f*]chromene derivatives: (a) The flow cytometry dot plot represents the Annexin-V-FITC staining in the X-axis and the PI in the Y-axis. The summary of the Annexin V-FITC apoptosis assay results displays the percentages of early apoptosis, late apoptosis, total apoptosis, and necrosis in the (b) MCF-7, (c) HCT-116, and (d) HepG-2 treated cells with the indicated drugs (IC₅₀ value) for 24 h. (e) The fold change of early and late apoptotic cells treated with compound 4e over the control.

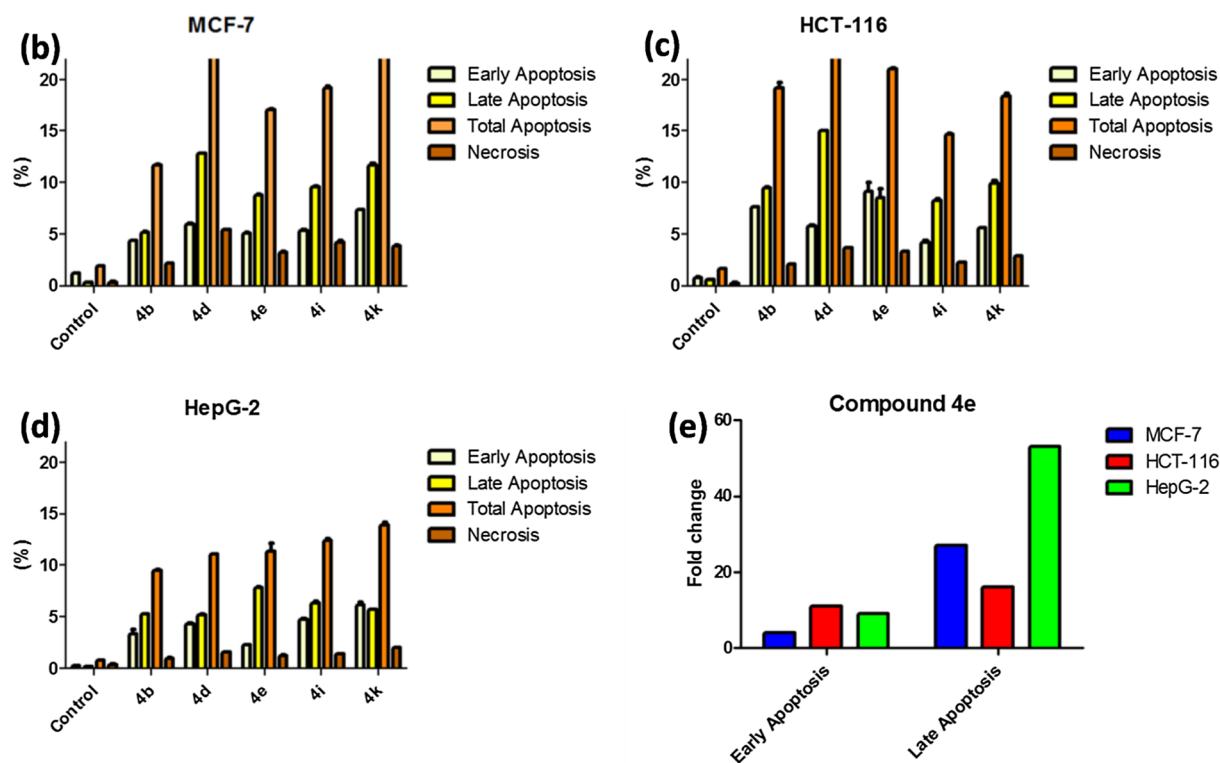


Fig. 5. (continued)

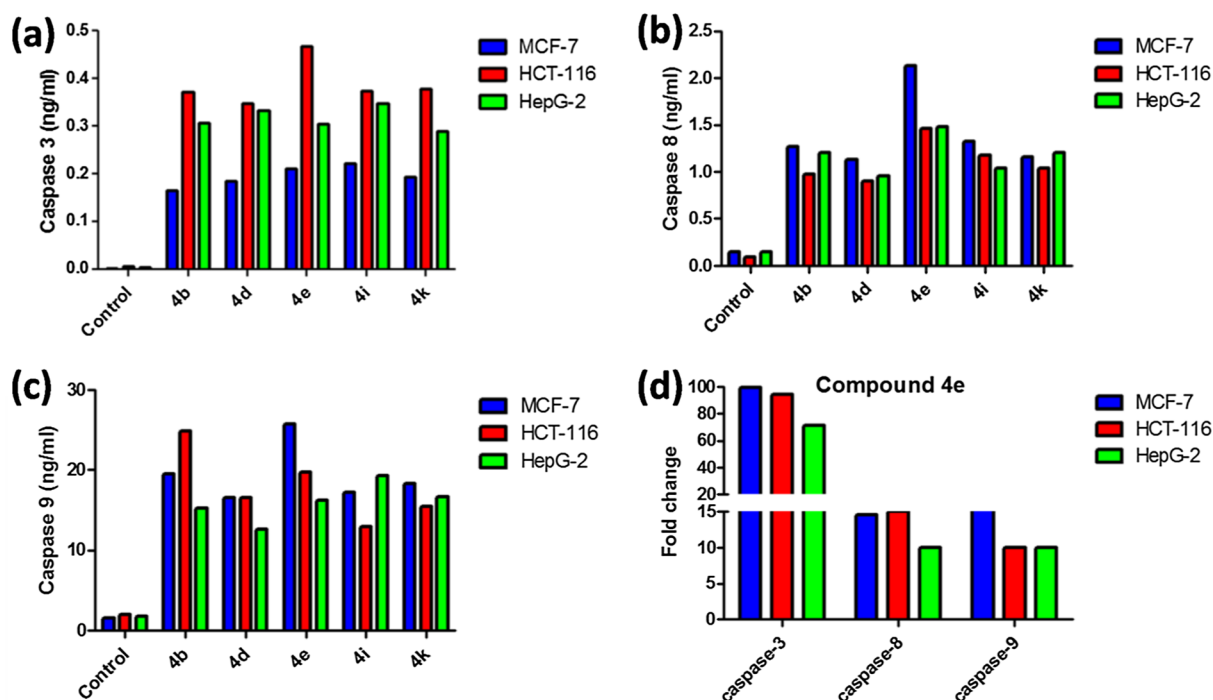


Fig. 6. Increased Caspase-3, -8, and -9 levels. The (a) Caspase-3, (b) Caspase-8, and (c) Caspase-9 concentration levels (ng/mL) in the different cell lysates were determined, using the enzyme-linked immunosorbent assay kit after the treatment of the tumor cells with the indicated compounds (IC_{50} value) for 24 h. (d) The fold change for Caspase-3, -8, and -9 in the treated cancer cells with compound 4e was calculated relative to the non-treated control cells.

study in assessment with Vinblastine, intimating that the halogenated disubstituents possessed excellent antiproliferative activities than the monosubstituents and trisubstituents. Furthermore, derivatives 4j, 4k, 4a, 4h, 4b, 4d, 4i, 4m, 4e, 4g, and 4l portrayed superior potency against the HepG-2 line in evaluation with Vinblastine, as compared to the monosubstituents members and the trisubstituent. Lastly, some of the selected derivatives of the assessed series demonstrated almost

equipotent to most potent antiproliferative activity in comparison to Doxorubicin in the treatment of the elected cell lines: the almost equipotent activity of compound 4d against MCF-7; the equipotent activity of compounds 4h, 4e and the almost equipotent activity of compounds 4k, 4d against Hct-116; and the most potent activity of compounds 4j, 4k, 4a and the equipotent activity of compounds 4b, 4h against HepG-2.

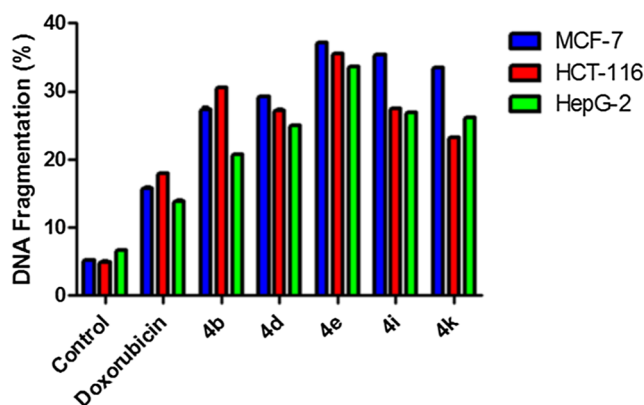


Fig. 7. Significant increased DNA fragmentation percentage in all treated cancer cells. The quantitative estimation of DNA fragmentation was discerned, using the diphenylamine (DPA) reagent. The percentage of DNA fragments in the cells treated with the indicated compounds was evaluated against the reference drug Doxorubicin.

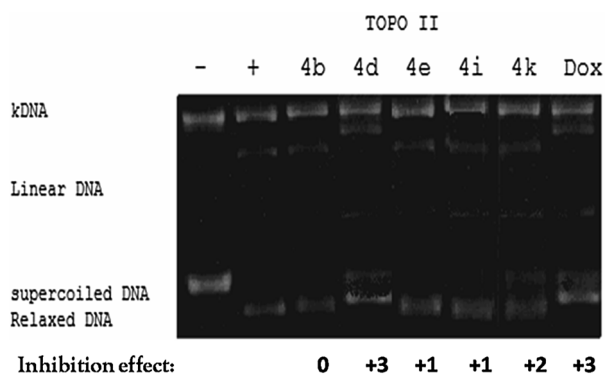


Fig. 8. The inhibition of the Topoisomerase II decatenation activity by the target compounds. The human topoisomerase II-mediated decatenation activity of kDNA was done, using the topoisomerase II inhibition gel assay. The (-) kDNA controls with no Topoisomerase II and the (+) decatenated kDNA controls with topoisomerase II. (0) No, (+1) low, (+2) moderate, and (+3) high inhibition effects.

3. Conclusion

This report portrays a novel and successful endeavor to develop halogenated 3-amino-1*H*-benzo[*f*]chromene derivatives and explore their dual inhibitory impact on the Topoisomerase II enzyme and microtubules with potent anticancer activities against three diverse cancer cell lines: MCF-7, HCT-116, and HepG-2. The dual inhibition of the Topoisomerase II/microtubules detains cells at the G2/M phases, activates extrinsic and intrinsic Caspase-dependent apoptosis, and, lastly, affords DNA fragmentation. Furthermore, the present study offers an innovative and efficacious strategy for cancer therapy by the dual targeting of the Topoisomerase II/microtubules to overcome the different medicinal problems encountered with the employment of the conventional combination of Topoisomerase II and tubulin inhibitors. Such strategy will also render the process of drug choice, administration, and potent therapeutic efficacy facilitated as well as simplified.

4. Experimental section

4.1. Materials and Equipment's

All chemicals were purchased from Sigma-Aldrich Chemical Co. (Sigma-Aldrich Corp., St. Louis, MO, USA). All the melting points were measured with a Stuart Scientific Co. Ltd apparatus, which are

uncorrected. The IR spectra were recorded on a KBr disc on a Jasco FT/IR 460 plus spectrophotometer. The ^1H (500 MHz), ^{13}C (125 MHz), and ^{19}F (377 MHz) NMR spectra were measured on a BRUKER AV 500 MHz spectrometer in $\text{DMSO-}d_6$, a solvent, using the tetramethylsilane (TMS) as an internal standard. The ^{13}C NMR spectra were obtained, employing the distortion-free enhancement by polarization transfer (DEPT) and the attached proton test (APT). The chemical shifts (δ) are expressed in parts per million (ppm). The Microwave apparatus utilized is Milestone Sr1, Microsynth. The mass spectra were determined on a Shimadzu GC/MS-QP5050A spectrometer. The elemental analysis was carried out at the Regional Centre for Mycology and Biotechnology (RCMP), Al-Azhar University, Cairo, Egypt, and the results were within $\pm 0.25\%$. The reaction courses and product mixtures were routinely monitored by the thin layer chromatography (TLC) on silica gel precoated F₂₅₄ Merck plates.

4.2. General procedure for synthesis of 1*H*-benzo[*f*]chromene derivatives (4*a*–4*m*) and 2-(2-Fluoro-4-(piperidin-1-yl)benzylidene)malononitrile (5)

A reaction mixture of 6-bromo-2-naphthol (**1**) (0.01 mol), different aromatic aldehydes (**2a–m**) (0.01 mol), malononitrile (**3**) (0.01 mol), and piperidine (0.5 mL) in an ethanol solution (30 mL) was heated under microwave irradiation conditions for 2 min. at 140 °C. After the reaction reached completion, the reaction mixture was cooled to room temperature, and the precipitated solid was filtered off, washed with methanol, and recrystallised from ethanol or ethanol/benzene. The physical and spectral data of compounds **4a–m** and **5** are as follows:

4.2.1. 3-Amino-8-bromo-1-(4-fluorophenyl)-1*H*-benzo[*f*]chromene-2-carbonitrile (4*a*)

Prepared as previously described [24].

4.2.2. 3-Amino-8-bromo-1-(2-chlorophenyl)-1*H*-benzo[*f*]chromene-2-carbonitrile (4*b*)

Colorless needles from ethanol; yield 87%; m.p. 255–256 °C; IR (KBr) ν (cm^{-1}): 3448, 3328, 3213 (NH_2), 2198 (CN); ^1H NMR ($\text{DMSO-}d_6$, 500 MHz) δ : 8.24–7.01 (m, 9H, aromatic), 7.02 (bs, 2H, NH_2), 5.71 (s, 1H, H-1); ^{13}C NMR ($\text{DMSO-}d_6$, 125 MHz) δ : 159.7 (C-3), 142.2 (C-4a), 132.1 (C-10a), 130.5 (C-7), 130.3 (C-9), 128.8 (C-6), 128.6 (C-6a), 124.9 (C-10), 119.7 (C-10b), 118.2 (CN), 118.1 (C-5), 115.0 (C-8), 56.1 (C-2), 35.2 (C-1), 147.5, 131.1, 130.1, 129.7, 129.2, 128.2 (aromatic); MS m/z (%): 414 ($\text{M}^+ + 4$, 3.11), 412 ($\text{M}^+ + 2$, 8.65), 410 (M^+ , 6.31) with a base peak at 299 (1 0 0); Anal. Calcd for $\text{C}_{20}\text{H}_{12}\text{BrClN}_2\text{O}$: C, 58.35; H, 2.94; N, 6.80. Found: C, 58.31; H, 2.91; N, 6.76%.

4.2.3. 3-Amino-8-bromo-1-(3-chlorophenyl)-1*H*-benzo[*f*]chromene-2-carbonitrile (4*c*)

Colorless needles from ethanol; yield 83%; m.p. 258–259 °C; IR (KBr) ν (cm^{-1}): 3449, 3327, 3219 (NH_2), 2199 (CN); ^1H NMR ($\text{DMSO-}d_6$, 500 MHz) δ : 8.20–7.05 (m, 9H, aromatic), 7.03 (bs, 2H, NH_2), 5.69 (s, 1H, H-1); ^{13}C NMR ($\text{DMSO-}d_6$, 125 MHz) δ : 159.8 (C-3), 142.2 (C-4a), 132.2 (C-10a), 130.4 (C-7), 130.3 (C-9), 129.1 (C-6), 128.7 (C-6a), 124.7 (C-10), 120.1 (C-10b), 118.3 (CN), 118.2 (C-5), 115.1 (C-8), 56.1 (C-2), 35.2 (C-1), 142.4, 135.1, 131.1, 129.6, 127.1 (aromatic); MS m/z (%): 414 ($\text{M}^+ + 4$, 3.14), 412 ($\text{M}^+ + 2$, 12.25), 410 (M^+ , 9.39) with a base peak at 299 (1 0 0); Anal. Calcd for $\text{C}_{20}\text{H}_{12}\text{BrClN}_2\text{O}$: C, 58.35; H, 2.94; N, 6.80. Found: C, 58.41; H, 3.00; N, 6.80%.

4.2.4. 3-Amino-8-bromo-1-(4-chlorophenyl)-1*H*-benzo[*f*]chromene-2-carbonitrile (4*d*)

Prepared as previously described [24].

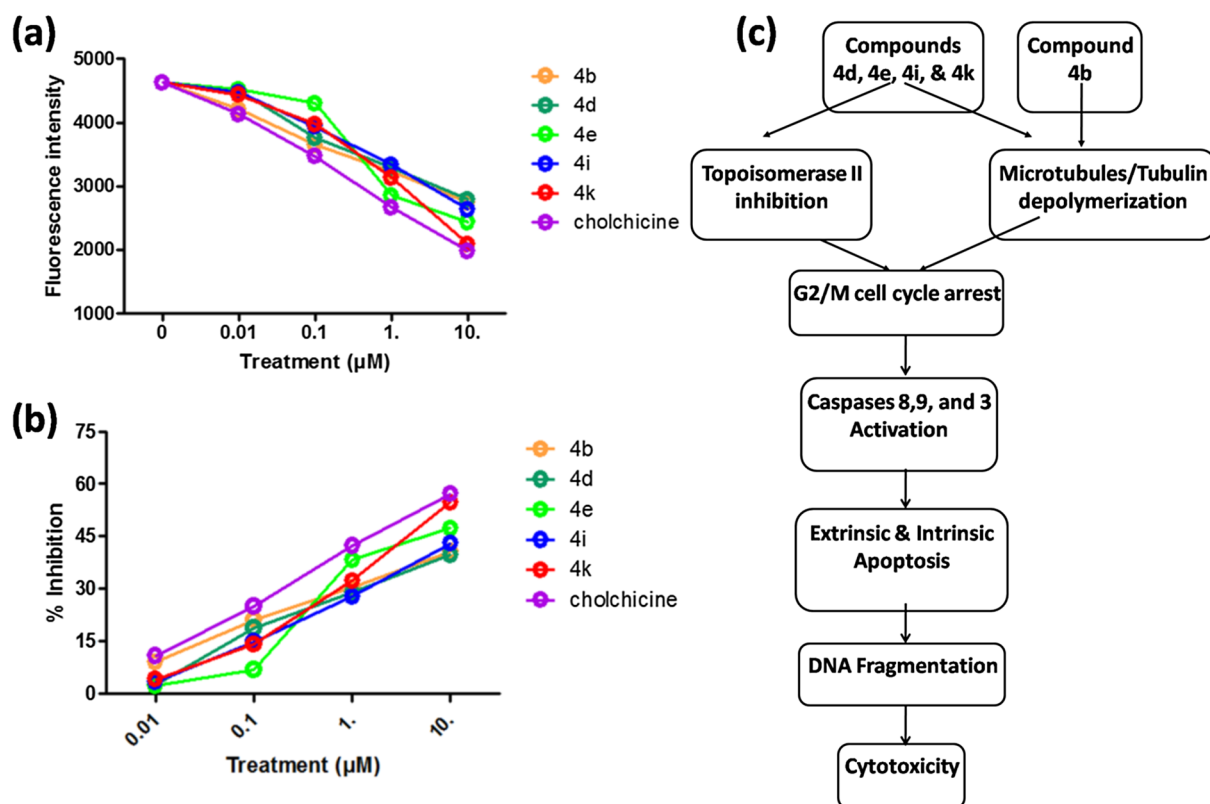


Fig. 9. The destabilization of the preformed microtubules by the target compounds in the cell-free system. (a) The dose response curves for the effect of the synthesized compounds **4b**, **4d**, **4e**, **4i**, and **4k** at four different concentrations (μM) on the depolymerization of the preformed microtubules, as monitored by the decrease in the fluorescence intensity. The excitation and emission wavelengths were 360 and 420 nm. (b) The graphical representation of the microtubules inhibition percentage of the different examined derivatives in comparison with Colchicine. (c) A schematic presentation of the possible mechanisms of action of the investigated compounds.

4.2.5. 3-Amino-8-bromo-1-(4-bromophenyl)-1H-benzo[f]chromene-2-carbonitrile (**4e**)

Prepared as previously described [24].

4.2.6. 3-Amino-8-bromo-1-(4-iodophenyl)-1H-benzo[f]chromene-2-carbonitrile (**4f**)

Colorless crystals from ethanol/benzene; yield 87%; m.p. 227–228 °C; IR (KBr) ν (cm^{-1}): 3448, 3318, 3181 (NH_2), 2201 (CN); ^1H NMR (DMSO- d_6 , 500 MHz) δ : 8.22–6.98 (m, 9H, aromatic), 7.05 (bs, 2H, NH_2), 5.32 (s, 1H, H-1); ^{13}C NMR (DMSO- d_6 , 125 MHz) δ : 159.5 (C-3), 147.1 (C-4a), 132.1 (C-10a), 130.3 (C-7), 130.0 (C-9), 129.0 (C-6), 128.8 (C-6a), 125.9 (C-10), 120.1 (C-10b), 118.2 (C-5), 118.1 (CN), 115.4 (C-8), 57.3 (C-2), 37.4 (C-1), 145.2, 137.5, 129.3, 92.6 (aromatic); MS m/z (%): 504 ($\text{M}^+ + 2$, 31.16) with a base peak at 502 (M^+ , 100); Anal. Calcd for $\text{C}_{20}\text{H}_{12}\text{BrIN}_2\text{O}$: C, 47.74; H, 2.40; N, 5.57. Found: C, 47.89; H, 2.54; N, 5.71%.

4.2.7. 3-Amino-8-bromo-1-(2,4-difluorophenyl)-1H-benzo[f]chromene-2-carbonitrile (**4g**)

Colorless crystals from ethanol; yield 66%; m.p. 300–301 °C; IR (KBr) ν (cm^{-1}): 3479, 3337, 3290 (NH_2), 2200 (CN); ^1H NMR (DMSO- d_6 , 500 MHz) δ : 8.63–7.05 (m, 8H, aromatic), 7.14 (bs, 2H, NH_2), 5.78 (s, 1H, H-1); ^{13}C NMR (DMSO- d_6 , 125 MHz) δ : 161.3 (C-3), 159.5 (C-4a), 147.1 (C-10a), 130.8 (C-7), 130.7 (C-9), 129.9 (C-6), 129.7 (C-6a), 129.5 (C-10), 128.6 (C-10b), 123.4 (C-5), 119.8 (C-8), 119.7 (CN), 53.7 (C-2), 28.6 (C-1), 160.1, 159.1, 131.1, 129.6, 117.2, 112.1 (aromatic); MS m/z (%): 414 ($\text{M}^+ + 2$, 16.63), 412 (M^+ , 17.73) with a base peak at 300 (1 0 0); Anal. Calcd for $\text{C}_{20}\text{H}_{11}\text{BrF}_2\text{N}_2\text{O}$: C, 58.13; H, 2.68; N, 6.78. Found: C, 58.18; H, 2.72; N, 6.82%.

4.2.8. 3-Amino-8-bromo-1-(2,6-difluorophenyl)-1H-benzo[f]chromene-2-carbonitrile (**4h**)

Colorless crystals from ethanol; yield 80%; m.p. 298–299 °C; IR (KBr) ν (cm^{-1}): 3453, 3338, 3224 (NH_2), 2190 (CN); ^1H NMR (DMSO- d_6 , 500 MHz) δ : 8.24–7.05 (m, 8H, aromatic), 7.16 (bs, 2H, NH_2), 5.68 (s, 1H, H-1); ^{13}C NMR (DMSO- d_6 , 125 MHz) δ : 161.1 (C-3), 159.1 (C-4a), 147.5 (C-10a), 131.9 (C-7), 130.6 (C-9), 129.8 (C-6), 129.8 (C-6a), 129.5 (C-10), 128.7 (C-10b), 124.0 (C-5), 119.9 (C-8), 119.6 (CN), 53.6 (C-2), 28.0 (C-1), 160.3, 159.1, 130.4, 118.1, 113.1, 112.3 (aromatic); MS m/z (%): 414 ($\text{M}^+ + 2$, 13.66), 412 (M^+ , 14.79) with a base peak at 300 (1 0 0); Anal. Calcd for $\text{C}_{20}\text{H}_{11}\text{BrF}_2\text{N}_2\text{O}$: C, 58.13; H, 2.68; N, 6.78. Found: C, 58.08; H, 2.63; N, 6.72%.

4.2.9. 3-Amino-8-bromo-1-(2,3-dichlorophenyl)-1H-benzo[f]chromene-2-carbonitrile (**4i**)

Colorless crystals from ethanol; yield 84%; m.p. 295–296 °C; IR (KBr) ν (cm^{-1}): 3448, 3329, 3213 (NH_2), 2193 (CN); ^1H NMR (DMSO- d_6 , 500 MHz) δ : 8.24–7.00 (m, 8H, aromatic), 7.18 (bs, 2H, NH_2), 5.78 (s, 1H, H-1); ^{13}C NMR (DMSO- d_6 , 125 MHz) δ : 159.8 (C-3), 144.8 (C-4a), 132.1 (C-10a), 130.5 (C-7), 130.4 (C-9), 128.8 (C-6), 128.7 (C-6a), 124.8 (C-10), 119.6 (C-10b), 118.3 (CN), 118.1 (C-5), 114.5 (C-8), 55.5 (C-2), 36.1 (C-1), 147.5, 132.1, 129.4, 129.2, 129.0, 124.8 (aromatic); MS m/z (%): 450 ($\text{M}^+ + 6$, 0.35), 448 ($\text{M}^+ + 4$, 2.54), 446 ($\text{M}^+ + 2$, 5.54), 444 (M^+ , 3.36) with a base peak at 300 (1 0 0); Anal. Calcd for $\text{C}_{20}\text{H}_{11}\text{BrCl}_2\text{N}_2\text{O}$: C, 53.84; H, 2.49; N, 6.28. Found: C, 53.90; H, 2.61; N, 6.40%.

4.2.10. 3-Amino-8-bromo-1-(2,4-dichlorophenyl)-1H-benzo[f]chromene-2-carbonitrile (**4j**)

Colorless crystals from ethanol; yield 82%; m.p. 297–298 °C; IR

(KBr) ν (cm⁻¹): 3448, 3330, 3210 (NH₂), 2193 (CN); ¹H NMR (DMSO-*d*₆, 500 MHz) δ : 8.23–7.02 (m, 8H, aromatic), 7.14 (bs, 2H, NH₂), 5.67 (s, 1H, H-1); ¹³C NMR (DMSO-*d*₆, 125 MHz) δ : 159.7 (C-3), 141.3 (C-4a), 132.1 (C-10a), 130.3 (C-7), 129.3 (C-9), 128.6 (C-6), 128.5 (C-6a), 124.8 (C-10), 119.5 (C-10b), 118.3 (CN), 118.1 (C-5), 114.4 (C-8), 55.6 (C-2), 34.8 (C-1), 147.5, 132.2, 132.0, 131.5, 130.5, 129.0 (aromatic); MS *m/z* (%): 450 (M⁺ + 6, 0.48), 448 (M⁺ + 6, 3.61), 446 (M⁺ + 2, 7.69), 444 (M⁺, 4.95) with a base peak at 300 (1 0 0); Anal. Calcd for C₂₀H₁₁BrCl₂N₂O: C, 53.84; H, 2.49; N, 6.28. Found: C, 53.95; H, 2.59; N, 6.39%.

4.2.11. 3-Amino-8-bromo-1-(2,5-dichlorophenyl)-1H-benzof[f]chromene-2-carbonitrile (4k)

Yellow crystals from ethanol; yield 81%; m.p. 293–294 °C; IR (KBr) ν (cm⁻¹): 3443, 3321, 3211 (NH₂), 2195 (CN); ¹H NMR (DMSO-*d*₆, 500 MHz) δ : 8.21–7.02 (m, 8H, aromatic), 7.17 (bs, 2H, NH₂), 5.67 (s, 1H, H-1); ¹³C NMR (DMSO-*d*₆, 125 MHz) δ : 159.8 (C-3), 144.2 (C-4a), 132.5 (C-10a), 130.6 (C-7), 129.5 (C-9), 128.6 (C-6), 128.8 (C-6a), 124.7 (C-10), 119.5 (C-10b), 118.3 (CN), 118.1 (C-5), 114.0 (C-8), 55.4 (C-2), 35.5 (C-1), 147.5, 132.0, 131.6, 130.4, 130.0, 128.8 (aromatic); MS *m/z* (%): 450 (M⁺ + 6, 1.35), 448 (M⁺ + 6, 9.54), 446 (M⁺ + 2, 22.54), 444 (M⁺, 13.36) with a base peak at 164 (1 0 0); Anal. Calcd for C₂₀H₁₁BrCl₂N₂O: C, 53.84; H, 2.49; N, 6.28. Found: C, 53.73; H, 2.39; N, 6.19%.

4.2.12. 3-Amino-8-bromo-1-(2,6-dichlorophenyl)-1H-benzof[f]chromene-2-carbonitrile (4l)

Colorless crystals from ethanol; yield 80%; m.p. 318–319 °C; IR (KBr) ν (cm⁻¹): 3447, 3326, 3210 (NH₂), 2195 (CN); ¹H NMR (DMSO-*d*₆, 500 MHz) δ : 8.21–7.28 (m, 8H, aromatic), 7.12 (bs, 2H, NH₂), 6.11 (s, 1H, H-1); ¹³C NMR (DMSO-*d*₆, 125 MHz) δ : 160.2 (C-3), 148.2 (C-4a), 134.3 (C-10a), 131.9 (C-7), 130.6 (C-9), 128.9 (C-6), 128.9 (C-6a), 124.6 (C-10), 119.3 (C-10b), 117.9 (CN), 117.8 (C-5), 112.7 (C-8), 52.7 (C-2), 35.0 (C-1), 137.1, 135.0, 131.0, 131.1, 129.8, 129.4 (aromatic); MS *m/z* (%): 450 (M⁺ + 6, 0.65), 448 (M⁺ + 6, 4.01), 446 (M⁺ + 2, 10.86), 444 (M⁺, 6.76) with a base peak at 300 (1 0 0); Anal. Calcd for C₂₀H₁₁BrCl₂N₂O: C, 53.84; H, 2.49; N, 6.28. Found: C, 53.90; H, 2.58; N, 6.35%.

4.2.13. 3-Amino-8-bromo-1-(3,5-dibromo-2-methoxyphenyl)-1H-benzof[f]chromene-2-carbonitrile (4m)

Colorless crystals from ethanol; yield 86%; m.p. 290–291 °C; IR (KBr) ν (cm⁻¹): 3443, 3320, 3209 (NH₂), 2202 (CN); ¹H NMR (DMSO-*d*₆, 500 MHz) δ : 8.22–7.19 (m, 7H, aromatic), 7.07 (bs, 2H, NH₂), 5.38 (s, 1H, H-1), 3.77 (s, 3H, OCH₃); ¹³C NMR (DMSO-*d*₆, 125 MHz) δ : 159.6 (C-3), 144.4 (C-4a), 132.1 (C-10a), 130.3 (C-7), 130.0 (C-9), 128.8 (C-6), 128.7 (C-6a), 125.9 (C-10), 120.1 (C-10b), 118.2 (CN), 118.1 (C-5), 115.5 (C-8), 57.3 (C-2), 55.2 (CH₃), 37.2 (C-1), 147.1, 131.3, 128.8, 112.8, 102.9 (aromatic); MS *m/z* (%): 450 (M⁺ + 6, 22.01), 566 (M⁺ + 4, 6.01), 564 (M⁺ + 2, 6.14), 562 (M⁺, 2.07) with a base peak at 300 (1 0 0); Anal. Calcd for C₂₁H₁₃Br₃N₂O₂: C, 44.64; H, 2.32; N, 4.96. Found: C, 44.71; H, 2.40; N, 5.05%.

4.2.14. 2-(2-Fluoro-4-(piperidin-1-yl)benzylidene)malononitrile (5)

Orange needles from ethanol; yield 32%; m.p. 222–223 °C (Lit. m.p. 224 °C; ³²); IR (KBr) ν (cm⁻¹): 2212 (CN); ¹H NMR (DMSO-*d*₆, 500 MHz) δ : 7.98 (t, 1H, Ph-H₃), 7.86 (s, 1H, =CH), 6.89 (dd, 1H, Ph-H₅), 6.79 (dd, 1H, Ph-H₆), 3.52, 3.37 (m, 4H, piperidinyl 2,6-CH₂), 1.63–1.56 (m, 6H, piperidinyl 3,4,5-CH₂); ¹³C NMR (DMSO-*d*₆, 125 MHz) δ : 150.0 (=CH), 116.30 (CN), 71.0 (C-1), 165.9, 156.4, 129.9, 115.59, 110.4, 98.8 (aromatic), 48.1, 25.6, 24.3 (piperidinyl); ¹³C NMR-APT (DMSO-*d*₆, 125 MHz) spectrum CH, CH₃ [positive (up)], CH₂, Cq [negative (down)], revealed the following signals at δ : 165.9 (aromatic ↓), 156.4 (aromatic ↓), 150.0 (=CH ↑), 129.9 (aromatic ↑), 116.3 (CN ↓), 115.5 (aromatic ↓), 110.4 (aromatic ↓), 98.8 (aromatic ↑), 71.0 (C-1 ↓), 48.1 (piperidinyl ↓), 25.6 (piperidinyl ↓), 24.3 (piperidinyl ↓); ¹⁹F NMR

(DMSO-*d*₆, 377 MHz) δ : -109.2 (Ar-F); MS *m/z* (%): 255 (M⁺, 12.07) with a base peak at 172 (1 0 0); Anal. Calcd for: C₁₅H₁₄FN₃: C, 70.57; H, 5.53; N, 16.46. Found: C, 70.46; H, 5.45; N, 16.38%.

4.2.15. Preparation of 2-(2-fluoro-4-(piperidin-1-yl)benzylidene)malononitrile (5) from 2-fluoro-4-piperidin-1-yl-benzaldehyde (7) and malononitrile (3)

Prepared as previously described [49].

4.3. Biological screening

4.3.1. Cell culture and cytotoxicity evaluation using viability assay

The derivatives **4a–m** was initially evaluated for their *in vitro* anti-tumor activities against three different human cell lines: MCF-7, HCT-116, and HepG-2. The *in vitro* cytotoxicity evaluation was performed at the Regional Center for Mycology & Biotechnology (RCMP), Al-Azhar University under different concentrations (50, 25, 12.5, 6.25, 3.125, 1.56, and 0 μg/mL); Vinblastine and Doxorubicin were employed as standard cytotoxic drugs. The measurements of cell growth and the *in vitro* cytotoxicity evaluation were determined, using the viability assay, as described in literature [29–31] and the results were cited in Table 1 and Fig. 3.

4.3.2. Cell cycle analysis

The cell cycle arrest distribution was performed, exploiting the Propidium Iodide Flow Cytometry Kit (ab139418, Abcam) as previously described [50]. The human cancer cell lines MCF-7, HCT-116, and HepG-2 at the 5 × 10⁴ cells were cultured in 60-mm dishes in the presence of various tested compounds with the concentration equal to the IC₅₀ values for 24 h. The cells were then harvested and fixed in a 100% ice cold ethanol at +4 °C for at least 2 h. After rewashing with PBS, the cells were incubated with a 200 μL 1X Propidium iodide (PI) + RNase Staining Solution for 30 min at room temperature in the dark. The DNA content in each cell nucleus was decided by a FACS Calibur flow cytometer (BD Biosciences, Franklin Lakes, NJ, and USA). The cell cycle phase distribution was analyzed, using the Cell Quest Pro software (BD Biosciences), which display the collected propidium iodide fluorescence intensity on FL2.

4.3.3. Annexin V-FITC apoptosis assay

The apoptosis assay was performed with an Annexin V-FITC/PI double staining apoptosis detection kit (K101, Biovision), exercising a flow cytometer [51]. The human cells treated with the different newly synthesized derivatives (IC₅₀ value) were harvested by the trypsinization, washed twice with 4 °C PBS, and re-suspended in the binding buffer. Subsequently, the Annexin V-FITC and Propidium iodide (PI) solutions were added to stain the cells before the analysis by the flow cytometry, where a minimum of 10,000 cells per sample were acquired. The Annexin V-FITC binding (FL1) and PI (FL2) were analyzed, using the Cell Quest Pro software (BD Biosciences).

4.3.4. Determination of Caspase-3, Caspase-8, and Caspase-9 production

Caspase-3, Caspase-8, and Caspase-9 protein levels, the cancer cells were treated with the investigated compounds (IC₅₀ value) and incubated for 24 h. Then, the Caspase-3, Caspase-8, and Caspase-9 concentrations level in the different cell lysates were verified, exploiting the enzyme-linked immunosorbent assay kit (KHO1091, BMS2024, and BMS2025; Invitrogen), according to the instructions of the manufacturer. The colored product was measured at 450 nm by a plate reader (ROBONIK P2000 Elisa Reader, Karnataka, India) after the reaction was terminated by the addition of the stop solution. The concentrations of the samples were calculated from the standard curve, and the results were presented as nanogram per milliliter (ng/mL). There was no cross-reactivity with the other Caspases.

4.3.5. DNA fragmentation

The DNA fragmentation was quantitatively established, through the means of the diphenylamine (DPA) reagent, according to the method of Boraschi and Maurizi [52]. The optical density was determined at 600 nm in the T (pellet with the intact DNA) and B (supernatant with fragmented DNA) fractions, to calculate the percentage of DNA fragmentation as follows:

$$\% \text{ Fragmented DNA} = T/T + B \times 100$$

4.3.6. Topoisomerase II inhibition gel assay

The Topoisomerase II Assay Kit (TG1001-1, TopoGEN) was carried out according to the manufacture instruction to discern if compounds (**4b**, **4d**, **4e**, **4i**, and **4k**) inhibited the catalytic decatenation activity of the topoisomerase II [53]. The decatenated reaction products were separated by the agarose gel electrophoresis prior to the photo documenting.

4.3.7. Destabilization of preformed microtubules

The altering microtubules polymerization was performed, employing the fluorescence-based *in vitro* tubulin polymerization assay kit (BK011, Cytoskeleton). In accordance with the manufacturer's instructions, the purified tubulin from the porcine brain (2 mg/mL) were polymerized efficiently in the assay buffer (80 mM PIPES, pH 6.9, 2 mM MgCl₂, 0.5 mM EGTA, 1 mM GTP, and 15% glycerol) at 37 °C to reach a maximum fluorescence after 30 min. After polymerization, the reaction mixtures were incubated with the increasing concentrations of the different tested molecules (0–10 μM) in 96-well microtiter plates. The fluorescence changes were measured in the Spectramax Gemini fluorescence plate reader (Molecular Devices, Sunnyvale, CA) at 37 °C, using excitation at 360 nm and emission at 420 nm. The destabilizing effect of our compounds on the preformed microtubules was measured as a decrease in the fluorescence intensity. The data were assessed against Colchicine, a standard microtubules destabilizer drug.

4.3.8. Statistics

All data were expressed as the means ± standard deviation (SD) from at least three independent experiments with similar results. The statistical analysis was performed by the GraphPad Prism 5.01 (GraphPad software, San Diego, CA, USA).

Declaration of Competing Interest

The authors declare that they have no known competing financial interests or personal relationships that could have appeared to influence the work reported in this paper.

Acknowledgements

The authors extend their appreciation to the Deanship of Science Research at King Khalid University, Saudi Arabia for funding this work through General Research Project under Grant Number (R.G.P.1/111/40). In addition, the author deeply thanks the Regional Center for Mycology & Biotechnology (RCMP), Al-Azhar University, Cairo, Egypt, for carrying out the antitumor study and elemental analyses.

Appendix A. Supplementary material

Supplementary data to this article can be found online at <https://doi.org/10.1016/j.bioorg.2019.103549>.

References

- [1] T.H. Afifi, R.M. Okasha, H.E.A. Ahmed, J. Ilas, T. Saleh, A.S. Abd-El-Aziz, Structure-activity relationships and molecular docking studies of chromene and chromene based azo chromophores: A novel series of potent antimicrobial and anticancer agents, *EXCLI J.* 16 (2017) 868–902.
- [2] D. Ashok, K.R. Srinivas, G. Velagapuri, H. Rao, Synthesis of pyrazolylfuro[2,3-*f*]chromenes and evaluation of their antimicrobial activity, *Chem. Het. Compd.* 52 (2016) 928–933.
- [3] N.D. Vala, H.H. Jardosh, M.P. Patel, 5-PS-TBD triggered general protocol for the synthesis of 4*H*-chromenes, pyrano[4,3-*b*]pyran and pyrano[3,2-*c*]chromene derivatives of 1*H*-pyrazole and their biological activities, *Chin. Chem. Lett.* 27 (2016) 168–172.
- [4] G. Singh, A. Sharma, H. Kaur, M. Ishar, Chromanyl-isoxazolidines as antibacterial agents: synthesis, biological evaluation, quantitative structure activity relationship, and molecular docking studies, *Chem. Biol. Drug. Des.* 87 (2016) 213–223.
- [5] A.M. Abdella, Y. Moatasim, M.A. Ali, A.H.M. Elwahy, I.A. Abdelhamid, Synthesis and anti-influenza virus activity of Novel bis(4*H*-chromene-3-carbonitrile) derivatives, *J. Het. Chem.* 54 (2017) 1854–1862.
- [6] Y.J. Rao, E.Y. Goud, Y. Hemasric, N. Jain, S. Gabriella, Synthesis and anti-proliferative activity of 6, 7-aryl/hetaryl coumarins, *Russ. J. Gen. Chem.* 86 (2016) 184–189.
- [7] A. Parthiban, M. Kumaravel, J. Muthukumar, R. Rukkumani, R. Krishna, H. Surya, P. Rao, Synthesis, *in vitro* and *in silico* anti-proliferative activity of 4-aryl-4*H*-chromene derivatives, *Med. Chem. Res.* 25 (2016) 1308–1315.
- [8] A.M. El-Agrody, A.H. Halawa, A.M. Fouda, A.M. Al-Dies, Antiproliferative activity of novel 4*H*-benzo[*h*]chromenes, 7*H*-benzo[*h*]chromeno[2,3-*d*]pyrimidines and the structure–activity relationships of the 2-, 3-positions and fused rings at the 2, 3-positions, *J. Saudi Chem. Soc.* 21 (2017) 82–90.
- [9] M. Azizmohammadi, M. Khoobi, A. Ramazani, S. Emami, A. Zarrin, O. Firuzi, R. Miri, A. Shafiee, 2*H*-chromene derivatives bearing thiazolidine-2,4-dione, rhodanine or hydantoin moieties as potential anticancer agents, *Eur. J. Med. Chem.* 59 (2013) 15–22.
- [10] V.N. Indulatha, N. Gopal, B. Jayakar, Anti-inflammatory activity of newly synthesised *N*-[4'-Oxo-2'-(substituted Aryl/Hetaryl)-Thiazolidin-3'-yl]-3-Carboxamido-2*H*-Chromen-2-one derivatives, *Int. J. Pharma. Technol. Res.* 3 (2011) 1930–1937.
- [11] I.J. Elenkov, B. Hrvacic, S. Markovic, M. Mesic, A.C. Klonkay, L. Lerman, A.F. Susic, I. Vujanovic, B. Bosnjak, K. Brajsa, D. Zihner, N.K. Hulita, I. Malnard, Synthesis and anti-inflammatory activity of novel furochromenes, *Croat. Chem. Acta.* 86 (2013) 253–264.
- [12] N. Kamdar, D. Haveliwala, P. Mistry, S. Patel, Design, synthesis and *in vitro* evaluation of antitubercular and antimicrobial activity of some novel pyranopyrimidines, *Eur. J. Med. Chem.* 45 (2010) 5056–5063.
- [13] A. Termentzi, I. Khouri, T. Gaslonde, S. Prado, B. Saint-Joanis, F. Bardou, E. Amanatiadou, I. Vizirianakis, J. Kordulkova, M. Jackson, R. Brosch, Y. Janin, M. Daff, F. Tillequin, S. Michel, Synthesis, biological activity, and evaluation of the mode of action of novel antitubercular benzofurobenzopyrans substituted on A ring, *Eur. J. Med. Chem.* 45 (2010) 5833–5847.
- [14] Y. Cui, M. Ao, W. Li, L. Yu, Effect of glabridin from *Glycyrrhiza glabra* on learning and memory in mice, *Planta Med.* 74 (2008) 377–380.
- [15] J. Ahn, H. Lee, J. Jang, S. Kim, T. Ha, Anti-obesity effects of glabridin-rich supercritical carbon dioxide extract of licorice in high-fat-fed obese mice, *Food Chem. Toxicol.* 4 (2012) 439–445.
- [16] D. Tiana, S. Dasa, J. Doshia, J. Peng, J. Lin, C. Xing, sHA 14–1, a stable and ROS-free antagonist against anti-apoptotic Bcl-2 proteins, bypasses drug resistances and synergizes cancer therapies in human leukemia cell, *Cancer Lett.* 259 (2008) 198–208.
- [17] D. Hermanson, S. Addo, A. Bajer, J. Marchant, S. Das, B. Srinivasan, F. Al-Mousa, F. Michelangeli, D. Thomas, T. LeBien, C. Xing, Dual mechanisms of sHA 14–1 in inducing cell death through endoplasmic reticulum and mitochondria, *Mol. Pharmacol.* 76 (2009) 667–678.
- [18] A. Parthiban, M. Kumaravel, J. Muthukumar, R. Rukkumani, R. Krishna, H.S.P. Rao, Synthesis, *in vitro* and *in silico* anti-proliferative activity of 4-aryl-4*H*-chromene derivatives, *Med. Chem. Res.* 25 (2016) 1308–1315.
- [19] Z. Saffari, H. Aryapour, A. Akbarzadeh, A. Foroumadi, N. Jafari, M.F. Zarabi, A. Farhangi, *In vitro* antitumor evaluation of 4*H*-chromene-3-carbonitrile derivatives as a new series of apoptotic inducers, *Tumor. Biol.* 35 (2014) 5845–5855.
- [20] J.-L. Wang, D. Liu, Z.-J. Zhang, S. Shan, X. Han, S.M. Srinivasula, C.M. Croce, S. Alnemri, Z. Huang, Structure-based discovery of an organic compound that binds Bcl-2 protein and induces apoptosis of tumor cells, *Proc. Natl. Acad. Sci. USA* 97 (2000) 7124–7129.
- [21] Y. Dai, M. Rahmani, S.J. Corey, P. Dent, S. Grant, A Bcr/Abl-independent, Lyn-dependent form of imatinib mesylate (STI-571) resistance is associated with altered expression of Bcl-2, *J. Biol. Chem.* 279 (2004) 34227–34239.
- [22] J.D. Lickliter, N.J. Wood, L. Johnson, G. McHugh, J. Tan, F. Wood, J. Cox, N.W. Wickham, HA14-1 selectively induces apoptosis in Bcl-2-overexpressing leukemia/lymphoma cells, and enhances cytarabine-induced cell death, *Leukemia* 17 (2003) 2074–2080.
- [23] D. Tian, S.G. Das, J.M. Doshi, J. Peng, J. Lin, C. Xing, sHA 14–1, a stable and ROS-free antagonist against anti-apoptotic Bcl-2 proteins, bypasses drug resistances and synergizes cancer therapies in human leukemia cell, *Cancer Lett.* 259 (2008) 198–208.
- [24] H.E.A. Ahmed, M.A.A. El-Nassag, A.H. Hassan, R.M. Okasha, S. Ihmaid, A.M. Fouda, T.H. Afifi, A.A. Aljuhani, A.M. El-Agrody, Introducing novel potent anticancer agents of 1*H*-benzo[*f*]chromene scaffolds, targeting c-Src kinase enzyme with MDA-MB-231 cell line anti-invasion effect, *J. Enzyme Inhib. Med. Chem.* 33 (2018) 1074–1088.
- [25] A. Rafinejad, A. Fallah-Tafti, R. Tiwari, A.N. Shirazi, D. Mandal, A. Shafiee, K. Parang, A. Foroumadi, T. Akbarzadeh, 4-Aryl-4*H*-naphthopyrans derivatives: one-pot synthesis, evaluation of Src kinase inhibitory and anti-proliferative activities, *Daru.* 20 (2012) 100–107.

- [26] C.P. Dell, Antiproliferative naphthopyrans: biological activity, mechanistic studies and therapeutic potential, *Curr. Med. Chem.* 5 (1998) 179–194.
- [27] H.E.A. Ahmed, M.A.A. El-Nassag, A.H. Hassan, H.M. Mohamed, A.H. Halawa, R.M. Okasha, S. Ihmaid, S.M. Abd El-Gilil, E.S.A.E.H. Khattab, A.M. Fouda, A.M. El-Agrody, A. Aljuhani, T.H. Affi, Developing lipophilic aromatic halogenated fused systems with specific ring orientations, leading to potent anticancer analogs and targeting the c-Src Kinase enzyme, *J. Mol. Struct.* 1186 (2019) 212–223.
- [28] A.M. Fouda, A.M. El-Agrody, A.E.-G.E. Amr, M.A. Al-Omar, H.A. Ghabbour, Spectroscopic Data, Single X-ray and Antimicrobial Activity of Microwave Synthesized 3-Amino-8-Bromo-1-(2,5-dichlorophenyl)-1*H*-Benzo[*f*]Chromene-2-Carbonitrile, *J. Comput. Theor. Nanosci.* 14 (2017) 3831–3836.
- [29] T. Mosmann, Rapid colorimetric assay for cellular growth and survival: application to proliferation and cytotoxicity assays, *J. Immunol. Methods* 65 (1983) 55–63.
- [30] M.I.C. Atta-ur-Rahman, W.J. Thomsen, *Bioassay Techniques for Drug Development*, Harwood Academic Publishers, 2001.
- [31] F. Demirci, K.H.C. Başer, *Bioassay Techniques for Drug Development By Atta-ur-Rahman, M. Iqbal Choudhary* (HEJRIC, University of Karachi, Pakistan), Thomsen, W. J. (Areana Pharmaceuticals, San Diego, CA). Harwood Academic Publishers, Amsterdam, The Netherlands, 2001.
- [32] G.K. Schwartz, M.A. Shah, Targeting the cell cycle: a new approach to cancer therapy, *J. Clin. Oncol.* 23 (2005) 9408–9421.
- [33] G.H. Williams, K. Stoeber, The cell cycle and cancer, *J. Pathol.* 226 (2012) 352–364.
- [34] V.A. Fadok, D.R. Voelker, P.A. Campbell, J.J. Cohen, D.L. Bratton, P.M. Henson, Exposure of phosphatidylserine on the surface of apoptotic lymphocytes triggers specific recognition and removal by macrophages, *J. Immunol.* 1 (1992) 2207–2222.
- [35] J.H. Liu, *Activation of Apoptosis Pathways by Different Classes of Anticancer Drugs*, University of Ulm, 2001.
- [36] Y.S. Tor, L.S. Yazan, J.B. Foo, N. Armania, Y.K. Cheah, R. Abdullah, M.U. Imam, N. Ismail, M. Ismail, Induction of apoptosis through oxidative stress-related pathways in MCF-7, human breast cancer cells, by ethyl acetate extract of *Dillenia suffruticosa*, *BMC Complement Altern. Med.* 14 (2014) 55–66.
- [37] S. Kumar, Regulation of caspase activation in apoptosis: implications in pathogenesis and treatment of disease, *Clin. Exp. Pharmacol. Physiol.* 26 (1999) 295–303.
- [38] G. Kroemer, S.J. Martin, Caspase-independent cell death, *Nat. Med.* 11 (2005) 725–730.
- [39] S.J. Seitz, E.S. Schleithoff, A. Koch, A. Schuster, A. Teufel, F. Staib, W. Stremmel, G. Melino, P.H. Kramer, T. Schilling, M. Muller, Chemotherapy-induced apoptosis in hepatocellular carcinoma involves the p53 family and is mediated via the extrinsic and the intrinsic pathway, *Int. J. Cancer* 126 (2010) 2049–2066.
- [40] R.U. Jänicke, M.L. Sprengart, M.R. Wati, A.G. Porter, Caspase-3 is required for DNA fragmentation and morphological changes associated with apoptosis, *J. Biol. Chem.* 273 (1998) 9357–9360.
- [41] B. Gabrielli, K. Brooks, S. Pavey, Defective cell cycle checkpoints as targets for anti-cancer therapies, *Front. Pharmacol.* 3 (2012) 9–14.
- [42] R.J. Isaacs, S.L. Davies, M.I. Sandri, C. Redwood, N.J. Wells, I.D. Hickson, Physiological regulation of eukaryotic topoisomerase II, *BBA-Gene Struct. Expr.* 1400 (1998) 121–137.
- [43] D.A. Nicholas, G. Brian, Topoisomerase II inhibitors and poisons, and the influence of cell cycle checkpoints, *Curr. Med. Chem.* 24 (2017) 1504–1519.
- [44] T.B.T. Magar, S.H. Seo, T.M. Kadayat, H. Jo, A. Shrestha, G. Bist, P. Katila, Y. Kwon, E.S. Lee, Synthesis and SAR study of new hydroxy and chloro-substituted 2,4-diphenyl-5*H*-chromeno[4,3-*b*]pyridines as selective topoisomerase II α -targeting anticancer agents, *Bioorg. Med. Chem.* 26 (2018) 1909–1919.
- [45] A.H. Corbett, N. Osheroff, When good enzymes go bad: conversion of topoisomerase II to a cellular toxin by antineoplastic drugs, *Chem. Res. Toxicol.* 6 (1993) 585–597.
- [46] E. Nogales, S.G. Wolf, K.H. Downing, Structure of the alpha beta tubulin dimer by electron crystallography, *Nature* 391 (1998) 199–203.
- [47] C. Dumontet, M.A. Jordan, Microtubule-binding agents: A dynamic field of cancer therapeutics, *Nat. Rev. Drug Discov.* 9 (2010) 790–803.
- [48] S. Bhattacharya, N.M. Kumar, A. Ganguli, M.P. Tantak, D. Kumar, G. Chakrabarti, NMK-TD-100, a novel microtubule modulating agent, blocks mitosis and induces apoptosis in HeLa cells by binding to tubulin, *PLoS ONE* 8 (2013) e76286, <https://doi.org/10.1371/journal.pone.0076286>.
- [49] E. Hendrickx, Y. Zhang, K.B. Ferrio, J.A. Herlocker, J. Anderson, N.R. Armstrong, E.A. Mash, A.P. Persoons, N. Peyghambarian, B. Kippelen, Photoconductive properties of PVK-based photorefractive polymer composites doped with fluorinated styrene chromophores, *J. Mater. Chem.* 9 (1999) 2251–2258.
- [50] L.L. Vindelov, L.J. Christensen, N.I. Nissen, Standardization of high-resolution flow cytometric DNA analysis by the simultaneous use of chicken and trout red blood cells as internal reference standards, *Cytometry* 3 (1983) 328–331.
- [51] G. Zhang, V. Gurtu, S.R. Kain, G. Yan, Early detection of apoptosis using a fluorescent conjugate of Annexin V, *Biotechniques* 23 (1997) 525–531.
- [52] D. Boraschi, G. Maurizi, Quantitation of DNA fragmentation with diphenylamine, in: D. Boraschi, P. Bossù, A. L'Aquila Cossarizza (Eds.), *Apoptosis - A Laboratory Manual of Experimental Methods*, GCI Publications, 1998, pp. 153–161.
- [53] B.M. Sahai, J.G. Kaplan, A quantitative decatenation assay for type II topoisomerases, *Anal. Biochem.* 156 (1986) 364–379.